Showcasing research from Professor Takato Mitsudome's laboratory, Graduate School of Engineering Science, Osaka University, Japan.

A cobalt phosphide catalyst for the hydrogenation of nitriles

A well-defined nano-cobalt phosphide serves as a new class of catalysts for the hydrogenation of nitriles to primary amines. While earth-abundant metal catalysts for nitrile hydrogenation generally suffer from air-instability (pyrophoricity), low activity and the need for harsh reaction conditions, nano-Co_2P shows both air-stability and high activity with an excellent turnover number exceeding 58000, which is over 500-fold greater than that of those previously reported. Moreover, nano-Co_2P efficiently promotes the hydrogenation of various nitriles to the corresponding primary amines even under an atmospheric pressure, far milder than the conventional reaction conditions.

ROYAL SOCIETY
OF **CHEMISTRY**

rsc.li/chemical-science

A cobalt phosphide catalyst for the hydrogenation of nitriles†

Takato Mitsudome, [ID] *[a] Min Sheng,[a] Ayako Nakata, [ID] [b] Jun Yamasaki,[c] Tomoo Mizugaki [ID] [a] and Koichiro Jitsukawa [ID] [a]

The study of metal phosphide catalysts for organic synthesis is rare. We present, for the first time, a well-defined nano-cobalt phosphide (nano-Co_2P) that can serve as a new class of catalysts for the hydrogenation of nitriles to primary amines. While earth-abundant metal catalysts for nitrile hydrogenation generally suffer from air-instability (pyrophoricity), low activity and the need for harsh reaction conditions, nano-Co_2P shows both air-stability and remarkably high activity for the hydrogenation of valeronitrile with an excellent turnover number exceeding 58000, which is over 20- to 500-fold greater than that of those previously reported. Moreover, nano-Co_2P efficiently promotes the hydrogenation of a wide range of nitriles, which include di- and tetra-nitriles, to the corresponding primary amines even under just 1 bar of H_2 pressure, far milder than the conventional reaction conditions. Detailed spectroscopic studies reveal that the high performance of nano-Co_2P is attributed to its air-stable metallic nature and the increase of the d-electron density of Co near the Fermi level by the phosphidation of Co, which thus leads to the accelerated activation of both nitrile and H_2. Such a phosphidation provides a promising method for the design of an advanced catalyst with high activity and stability in highly efficient and environmentally benign hydrogenations.

Introduction

The development of efficient, sustainable and cost-effective chemical processes is one of the ultimate goals of chemical research in both academia and industry. In this regard, the advance of catalytic hydrogenation processes of carboxylic acid derivatives is a major step towards developing green technology for producing numerous valuable chemicals and fuels.[1,2] In particular, the hydrogenation of nitriles represents a significantly important and straightforward method with 100% atomic efficiency for the synthesis of primary amines, which are ubiquitous motifs and are widely used in industry as solvents, surfactants, polymer intermediates, dyes, and important building blocks for pharmaceuticals.[3–5] In industrial nitrile hydrogenation processes, earth-abundant metal catalysts, Ni and Co-based sponge metals (RANEY® catalysts), have been mainly employed.[6] However, these metallic (zero-valent)

catalysts have the fatal issue of air instability (pyrophoricity), which results in the difficulty of catalyst handling,[7] and thus makes the chemical processes complicated. Furthermore, these catalysts show low activity, requiring harsh reaction conditions such as high H_2 pressures (200–400 bar) with limited substrate scope, and tend to significantly deactivate during storage.[8]

Hydrogenation of nitriles is facilitated by precious metal catalysts mainly based on Pt,[9–11] Ru,[12] Rh,[13,14] Re[15] and Ir.[16] These catalysts are active under mild conditions; nevertheless, the constituent metals are expensive and rare. Alternatively, some improvements using homogeneous earth-abundant metal catalysts have been reported.[17–26] However, these catalysts still require high H_2 pressures and have practical drawbacks, such as difficulty of catalyst recovery and reuse, the need for synthetically complex ligands and the contamination risk of dissolved metals. Heterogeneous catalysts have numerous advantages over homogeneous catalysts, which include their high durability, facile separation from the reaction mixture and subsequent reusability. In recent studies on heterogeneous catalysts, surface modification of metal nanoparticles by pyrolysis, as a means to improve air stability, was successfully explored.[27–31] The pyrolysis of metal–nitrogen complexes[27–30] and metal–organic frameworks (MOFs)[31] can provide Co and Ni nanoparticles with an N-doped carbon layer, which serve as air-stable and reusable catalysts for nitrile hydrogenation. However, owing to the shielding of surface active sites by the carbon coating, the air stability comes at the expense of activity,

[a] *Department of Materials Engineering Science, Graduate School of Engineering Science, Osaka University, 1-3 Machikaneyama, Toyonaka, Osaka 560-8531, Japan. E-mail: mitsudom@cheng.es.osaka-u.ac.jp*

[b] *First-principles Simulation Group, Nano-Theory Field, International Center for Materials Nanoarchitectonics (WPI-MANA), National Institute for Materials Science (NIMS), 1-1 Namiki, Tsukuba, Ibaraki 305-0044, Japan*

[c] *Research Center for Ultra-High Voltage Electron Microscopy, Osaka University, 7-1 Mihogaoka, Ibaraki, Osaka 567-0047, Japan*

† Electronic supplementary information (ESI) available. See DOI: 10.1039/d0sc00247j

and these state-of-the-art catalysts still suffer from insufficient activity with a turnover number (TON) of less than 62.[28] Therefore, earth-abundant metal heterogeneous catalysts with both high stability and activity have not yet been developed,[32] and the establishment of a promising means to break the trade-off between air stability and activity remains a great challenge.

Herein, we show that the nano-sized cobalt phosphide (nano-Co_2P) serves as a highly efficient heterogeneous catalyst for nitrile hydrogenation under mild conditions. The well-defined nano-Co_2P catalyst has a unique metallic nature with air stability and shows a remarkably high activity with an excellent TON exceeding 58000. Moreover, nano-Co_2P is shown, for the first time, to promote the ambient pressure hydrogenation of various aromatic and aliphatic nitriles, including di- and tetra-nitriles, which represents a breakthrough in overcoming the limitations of conventional catalysts. Metal phosphides are less common metals that extend beyond traditional metal (0) and metal oxide materials. Although metal phosphides have recently emerged as new electro- and photo-catalysts for the hydrogen evolution reaction[33–37] and hydrotreatment catalysts in the petroleum industry,[38–41] their catalysis for organic synthesis remains largely unexplored despite their unique characteristics.[42–46] Therefore, nano-Co_2P reported here can be categorized as a new class of catalyst for the hydrogenation of nitriles that is quite different from conventional catalysts of modified metal nanoparticles, sponge metals and metal complexes.

Results and discussion

Preparation and characterization of nano-Co_2P

A nano-Co_2P was newly synthesized based on a previous report with some modifications.[47] Briefly, $CoCl_2 \cdot 6H_2O$ was added to 1-octadecene in the presence of hexadecylamine and triphenylphosphite. The mixture was then stirred with increasing the temperature to 300 °C under an Ar atmosphere, which gave a black colloidal solution. The precipitate was collected by centrifugation and washed with acetone and chloroform, affording the nano-Co_2P. Transmission electron microscope (TEM) images of the obtained nano-Co_2P from the side view showed that nanorods with an average size of 20 × 9 nm (length × width) were regularly formed (Fig. 1a) and the hexagonal phase of nano-Co_2P was observed from the top view (Fig. 1b). The rod-length of nano-Co_2P is slightly shorter than the 33 nm length of Co_2P previously reported.[47] The high-resolution TEM (HRTEM) image further revealed that lattice fringes with a d-spacing of 0.22 nm corresponded to the (121) plane of the di-cobalt phosphide (Co_2P) and the selected area electron diffraction (SAED) pattern (Fig. 1c inset) showed that the diffraction rings were indexed to (121), (002), (312) and (322) planes of the Co_2P crystal, in agreement with the XRD pattern (Fig. S3a†).[48] Scanning transmission electron microscope (STEM) with elemental mapping of nano-Co_2P confirmed the presence of the constituent elements cobalt and phosphorus, which were distributed homogeneously within each nano-Co_2P (Fig. 1d–f). The corresponding energy dispersive X-ray (EDX) spectrum also revealed that the atomic ratio between Co and P was close to 2 : 1. All these results strongly demonstrated the successful
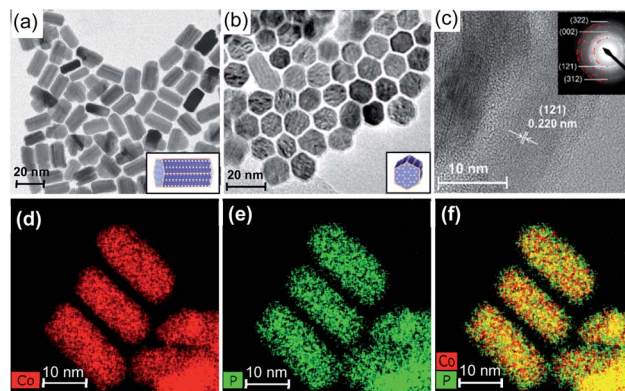

Fig. 1 (a) Side view TEM image of nano-Co_2P showing a nanorod morphology. (b) Top view TEM image of nano-Co_2P showing the hexagonal phase structure. (c) HRTEM image of nano-Co_2P with a SAED pattern (inset). Elemental mapping images of (d) Co and (e) P. (f) Composite overlay image formed from (d) and (e).

synthesis of a nano-sized Co_2P. The fabricated nano-Co_2P was stable and could be treated in air.

Catalytic performance of nano-Co_2P in nitrile hydrogenation

The catalytic activity of various metal phosphides was investigated in the hydrogenation of valeronitrile (**1a**) as a model substrate in the presence of NH_3 aq. under an H_2 pressure of 40 bar at 130 °C without any catalyst treatment before the reaction. The results are shown in Fig. 2a. It is noted that nano-Co_2P exhibited high catalytic activity, which produced the corresponding amine (**1b**) in high yield. Nano-cobalt phosphide with different compositions, nano-CoP also promoted the hydrogenation, giving a lower yield of **1b** compared with nano-Co_2P. In sharp contrast to Co_xP (x = 1 or 2), other Ni-, Cu-, and Fe-based metal phosphides showed poor activity. Furthermore, the Co nanoparticles (NPs) without phosphidation, CoO_x NP and bulk Co_2P, were hardly active. These results clearly showed a specific behavior of nano-Co_xP that was distinguished from the other metal phosphides and the conventional Co catalysts. This work is the first demonstration of a metal phosphide capable of the hydrogenation of carboxylic acid derivatives. The incorporation
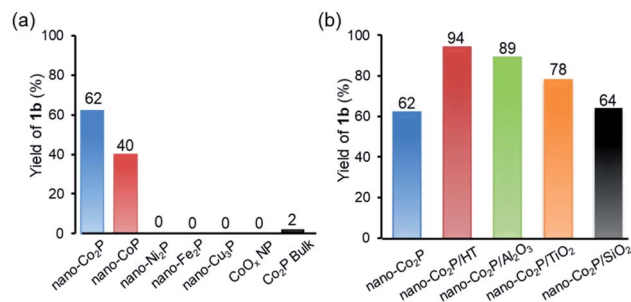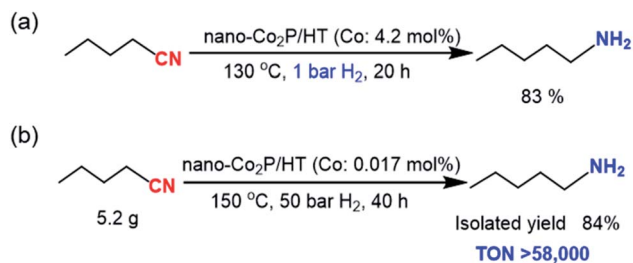

Fig. 2 (a) Catalytic performance of various metal phosphides and Co oxide nanoparticles in the hydrogenation of **1a**. (b) Catalytic performance of nano-Co_2P and nano-Co_2P on different supports. Reaction conditions: catalyst (metal: 4.2 mol%), **1a** (0.5 mmol), 2-propanol (3 mL), NH_3 aq. (1.2 mL), 130 °C, 40 bar H_2, 1 h.

Scheme 1 (a) Hydrogenation of **1a** under ambient pressure of H_2. (b) Gram scale experiment.

of phosphorus atoms into cobalt generated high catalytic activity for nitrile hydrogenation.

To evaluate the support effects of nano-Co_2P with the highest activity, nano-Co_2P supported on various materials was investigated in the hydrogenation of **1a** (Fig. 2b). Co_2P dispersed on supports all showed an improved activity from nano-Co_2P itself in the yield of **1b** owing to the increase of surface area of Co_2P by dispersion. Hydrotalcite (HT: $[Mg_6Al_2(OH)_{16}]CO_3 \cdot 4H_2O$) was the best support among various materials.

With the optimized nano-Co_2P/HT catalyst in hand, the catalytic performance was investigated under several reaction conditions. Remarkably, the high activity was demonstrated under much milder reaction conditions, with the hydrogenation of **1a** proceeding to give a high yield of **1b** even when the H_2 pressure was decreased to just 1 bar (Scheme 1a). This is the first example of an earth-abundant metal catalyst promoting ambient pressure hydrogenation of nitriles. Furthermore, increasing the nitrile amounts to 5.0 g resulted in a high yield production of **1b** with excellent TON exceeding 58000 based on the active surface Co atoms of nano-Co_2P. This TON value is over 20- to 500-fold greater than those of the homogeneous and heterogeneous earth-abundant catalysts developed to date (Table S2†), which demonstrates the high activity and stability of this catalyst even under prolonged heating at elevated temperatures (Scheme 1b).

After the reaction, nano-Co_2P/HT was easily recovered and proved to be reusable without any catalyst pre-treatment unlike
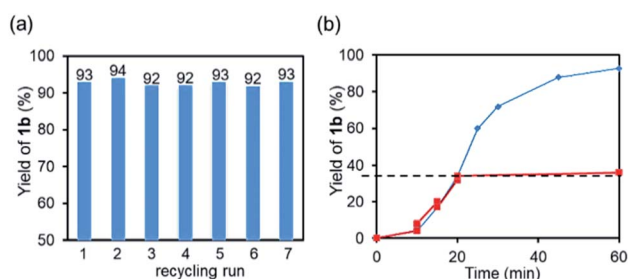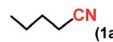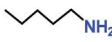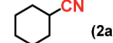
previous reports[29] and retained its high activity and selectivity even after the 7th reuse (Fig. 3a). The initial reaction rate was also maintained during the reuse experiments (Fig. S4†). Furthermore, the TEM image of the used nano-Co_2P/HT showed that the rod-structure of nano-Co_2P with an average size of 26 × 8 nm (length × width) was very similar to that of the fresh one, revealing the high durability of nano-Co_2P (Fig. S1†). To determine whether the hydrogenation proceeded heterogeneously, nano-Co_2P/HT was removed from the reaction mixture by

Table 1 Hydrogenation of nitriles using the nano-Co_2P/HT catalyst[a]

		$R-CN \xrightarrow[\text{40 bar } H_2, 130\,°C]{\text{nano-}Co_2P/HT \text{ (Co: 4.2 mol%)}} R \diagdown NH_2$		
Entry	Substrate	Time (h)	Product	Yield[b] (%)
1	(1a)	1	(1b)	94 (93)[c]
2	(2a)	2	(2b)	99 (82)[c]
3	C_8H_{17} CN (3a)	4	C_9H_{19} NH_2 (3b)	88
4	(4a)	4	(4b)	91 (84)[c]
5	(5a)	1	(5b)	93 (89)[c]
6	(6a)	1	(6b)	99
7	(7a)	2	(7b)	92
8	(8a)	5	(8b)	92 (85)[c]
9	(9a)	4	(9b)	95 (88)[c]
10	(10a)	2	(10b)	93
11	MeO (11a)	1	MeO (11b)	93 (87)[c]
12	Br (12a)	2	Br (12b)	92 (83)[c]
13	F_3C (13a)	2	F_3C (13b)	90 (90)[c]
14	(14a)	2	(14b)	94
15[d]	(15a)	5	(15b)	88 (87)[c]

[a] Reaction conditions: nano-Co_2P/HT (0.1 g), substrate (0.5 mmol), 2-propanol (3 mL), NH_3 aq. (1.2 mL). [b] Determined by GC using biphenyl as the standard. [c] Isolated yield as a hydrochloride salt. [d] NH_3 aq. (0.4 mL). All the substrates achieved complete conversions. Less than 5% alcohol and amide were detected as byproducts.

Fig. 3 (a) Reuse experiments of nano-Co_2P/HT in the hydrogenation of **1a** to **1b**. (b) Hot filtration experiment of nano-Co_2P/HT in the hydrogenation of **1a** to **1b**. (blue line) In the presence of nano-Co_2P/HT, and (red line) remove nano-Co_2P/HT at 20 min. Reaction conditions: nano-Co_2P/HT (0.1 g), **1a** (0.5 mmol), 2-propanol (3 mL), NH_3 aq. (0.8 mL), 130 °C, 40 bar H_2, 1 h.

Edge Article
Chemical Science

filtration at 35% yield of **1b**. The filtrate was again treated under hydrogen reaction conditions, and provided no forma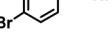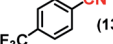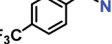tion of additional amine products, which clearly supported that the above hydrogenation occurred on the Co_2P surface (Fig. 3b).

Next, the nano-Co_2P/HT catalyst was examined for the hydrogenation of various nitriles. The results summarized in Table 1 demonstrate the remarkably wide scope of this catalyst: aliphatic (Table 1, entries 1–4) and aromatic nitriles (Table 1, entries 5–15), including benzonitriles having electron withdrawing or donating groups, were efficiently converted to the corresponding primary amines in high yields. Heteroaromatic nitriles, including nitrogen and oxygen atoms, were also good substrates and the desired amines were obtained in high yields (Table 1, entries 7–10). Furthermore, nano-Co_2P was evaluated in the chemoselective hydrogenation of nitriles containing easily reducible functional groups, which is known as a highly challenging objective because of its low functional group tolerance.[18] Notably, nano-Co_2P showed high chemoselectivity: functional groups, such as ketone and ester moieties, were tolerant, and gave the corresponding amines in high yields (Table 1, entries 14 and 15).

Nano-Co_2P/HT was also applicable to the hydrogenation of multinitriles (Scheme 2). Adiponitrile was hydrogenated to 1,6-hexamethylenediamine (**16b**), which is an important building block for the production of Nylon-6,6. Sebaconitrile, which can be obtained from biomass derivatives,[49] was converted selectively to 1,10-diaminodecane (**17b**). Aromatic dinitriles, terephthalonitrile and isophthalonitrile sufficiently provided diamines (**18b** and **19b**). A tetra-nitrile, 3,3′,3″,3‴-(butane-1,4-diyldinitrilo)tetrapropanenitrile, was also sufficiently transformed to its corresponding amine with all CN end groups hydrogenated (**20b**).

Moreover, various nitriles underwent an atmospheric pressure hydrogenation in the presence of nano-Co_2P/HT, giving excellent yields of amines (Scheme 3), which demonstrated the generality and the high catalytic performance of nano-Co_2P.

To investigate the origin of the unique catalytic properties of nano-Co_2P, X-ray absorption fine structure (XAFS) analysis was carried out under an air atmosphere. The Co K-edge X-ray absorption near edge structure (XANES) spectra of nano-CoP
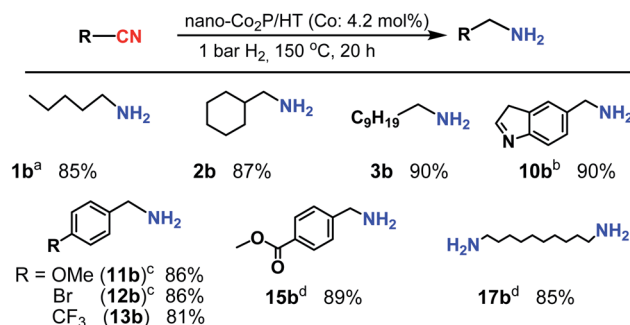
Scheme 3 Hydrogenation of nitriles using the nano-Co_2P catalyst under ambient pressure of H_2. Reaction conditions: nano-Co_2P/HT (0.1 g), substrate (0.5 mmol), 2-propanol (3 mL), NH_3 aq. (1.2 mL) and yield determined by GC using biphenyl as the standard. [a] 130 °C. [b] NH_3 aq. (0.6 mL). [c] 16 h. [d] Nano-Co_2P/HT (0.2 g), NH_3 aq. (0.6 mL).

and nano-Co_2P exposed in air are depicted in Fig. 4a. The absorption edge energies were much lower than that of CoO and very similar to that of Co foil, which suggested that the Co species in nano-CoP and nano-Co_2P represented metallic states even under atmospheric conditions.[50] Fourier transformation (FT) of the k^3-weighted extended X-ray adsorption fine structure (EXAFS) data of nano-CoP and nano-Co_2P showed two main peaks around 1.8 and 2.3 Å, which were attributed to Co–P and Co–Co scattering,[51] respectively (Fig. 4b). A metallic nature with hydrogenation ability of nano-Co_2P can be derived from the construction of the metal–metal bond.[52] The higher peak intensity of the Co–Co bond of nano-Co_2P than nano-CoP may account for the superior activity of nano-Co_2P to nano-CoP in the nitrile hydrogenation.[53]

The electronic state of surface Co in nano-Co_2P was also investigated by X-ray photoelectron spectroscopy (XPS). The Co 2p spectrum of nano-Co_2P showed a typical pair of Co $2p_{3/2}$ and Co $2p_{1/2}$ (Fig. 5a). The Co $2p_{3/2}$ and $2p_{1/2}$ binding energy peaks were located dominantly at 777.7 eV and 792.9 eV, respectively, which were very close to those of metallic Co $2p_{3/2}$ (777.9 eV) and $2p_{1/2}$ (793.5 eV). Thus, there were reduced Co species in the nano-Co_2P surface that were partially negatively charged ($Co^{\delta-}$). These data are consistent with the XANES results (Fig. 4a).[54] The XPS spectrum of P 2p showed an asymmetric peak, which could
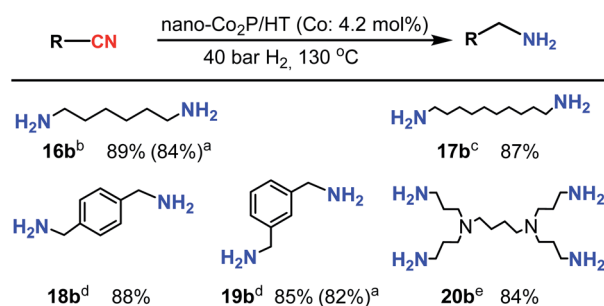
Scheme 2 Hydrogenation of multinitriles using the nano-Co_2P catalyst. Reaction conditions: nano-Co_2P/HT (0.1 g), substrate (0.5 mmol), 2-propanol (3 mL), NH_3 aq. (1.2 mL), yield determined by GC using biphenyl as the standard. [a] Isolated yield as a hydrochloride salt. [b] NH_3 aq. (0.6 mL), 4 h. [c] 4 h. [d] 10 h. [e] Substrate (0.07 mmol), 100 °C, 50 bar H_2, 3 h and yield determined by NMR using biphenyl as the standard.
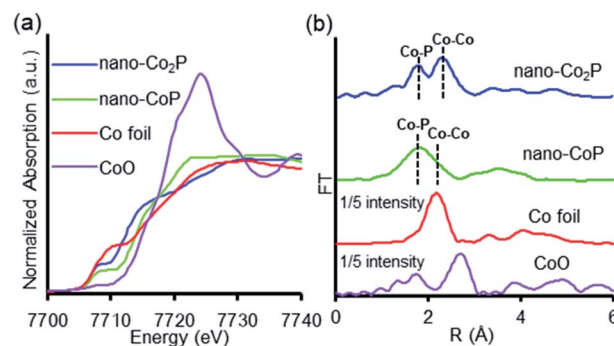

Fig. 4 (a) Co K-edge XANES spectra of nano-Co_2P, nano-CoP, Co foil, and CoO. (b) Fourier transformation of the k^3-weighted EXAFS of nano-Co_2P, nano-CoP, Co foil, and CoO.
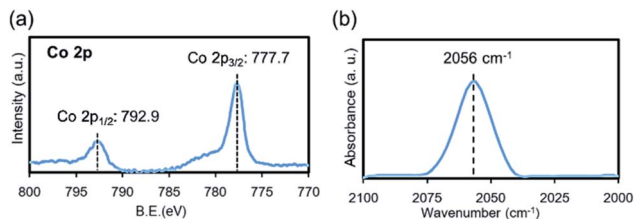
Fig. 5 (a) Co 2p XPS spectrum of nano-Co_2P. (b) *In situ* FT-IR spectroscopy of CO adsorption on nano-Co_2P.

be split into two peaks located at 129.0 and 130.0 eV attributed to P $2p_{3/2}$ and P $2p_{1/2}$ in Co_2P,[55] and another peak that split into two peaks located at 133.3 and 134.4 eV, which represented the phosphate species due to the surface oxidation (Fig. S5†).[56]

FT-IR spectroscopy of CO adsorption is another important tool to investigate the electronic state of Co. Fig. 5b shows the FT-IR spectrum of CO chemisorption on nano-Co_2P. An absorption band was observed at 2056 cm^{-1}, which lay at lower frequencies than that of gaseous CO (2143 cm^{-1}) owing to the back-donation of electrons to the $2\pi^*$ antibonding molecular orbital of CO. This red-shift was attributed to CO linearly adsorbed on an electron-populated cobalt center.[57]

Taken as a whole, these results clearly showed that nano-Co_2P has an air-stable metallic nature ($Co^{\delta-}$) much different from the conventional earth-abundant metals (0) with air instability. Therefore, nano-Co_2P enables easy catalyst handling with a safety in air and no requirement for pre-treatment with H_2 at high temperatures before the hydrogenation.

Finally, the structure–activity relationship of nano-Co_2P was investigated by the density functional theory (DFT) calculations (see the ESI† for DFT calculation details). Fig. 6a and b show the projected density of states (PDOS) of Co d-orbitals in bulk Co, bulk Co_2P, and Co_2P (0001) surfaces, and their differences, respectively. It is noted that Co atoms at the Co_2P surface exhibited larger amplitudes of the d-orbital PDOS around the Fermi level compared with the Co atoms both in the bulk Co and in bulk Co_2P.[58] This increase of the d-electrons around the Fermi level favors the donation of the electrons to the lowest unoccupied molecular orbital (LUMO) of nitrile, which dissociates the C≡N bond.[59] We also investigated H_2 dissociation around the Co atoms at the Co_2P surface. The H_2 molecule at the hollow site of the Co_2P was dissociated, where the distance between two H atoms was increased from 0.79 Å to 2.02 Å (Fig. 6d). The dissociative adsorption energy of H_2 on the Co_2P surface was calculated to be 26 kcal mol^{-1}, which was larger than that on the Co surface.[60] This indicated that Co_2P enhanced the H_2 dissociation compared with Co metal through the electron transfer from Co_2P to the σ^* orbital of H_2. These calculation results well support the high activity of nano-Co_2P in the hydrogenation of nitriles, where the increase of the d-electrons in nano-Co_2P would enhance the back-donation to the π^* orbital of nitrile, which weakens the C≡N bond. The activated C≡N bond may easily be hydrogenated by the dissociatively adsorbed hydrogen at the Co site.

Conclusions

We report a new, general and green sustainable methodology for producing primary amines from nitriles by developing a well-defined nano-Co_2P catalyst. The fabricated nano-Co_2P uniquely has air stability and high catalytic activity for a wide range of nitriles to the corresponding primary amines under mild conditions. Typically, the catalyst could be operated under an H_2 pressure of just 1 bar, far milder than the conventional harsh reaction conditions, which represents the first example of an earth-abundant metal catalyst for ambient pressure hydrogenation of nitriles. XAFS and DFT calculations reveal that the nano-Co_2P catalyst originally has a metallic nature with a high d-electron density of Co, which leads to high activity with air stability through the accelerated activation of both nitrile and H_2. Our findings not only provide a new category of nitrile hydrogenation catalysts, but also represent the first attempt to use metal phosphides as air-stable heterogeneous catalysts for the hydrogenation of carboxylic acid derivatives, which might lead to a new paradigm in the development of efficient, sustainable and cost-effective hydrogenation of various compounds, especially other carboxylic acid derivatives.

Experimental

Materials

All precursors and solvents were used as received, without further purification. $CoCl_2 \cdot 6H_2O$ and 1-octadecene (technical grade 90%) were purchased from Nacalai Tesque, Inc., and Sigma-Aldrich. Co. Hexadecylamine and triphenyl phosphite
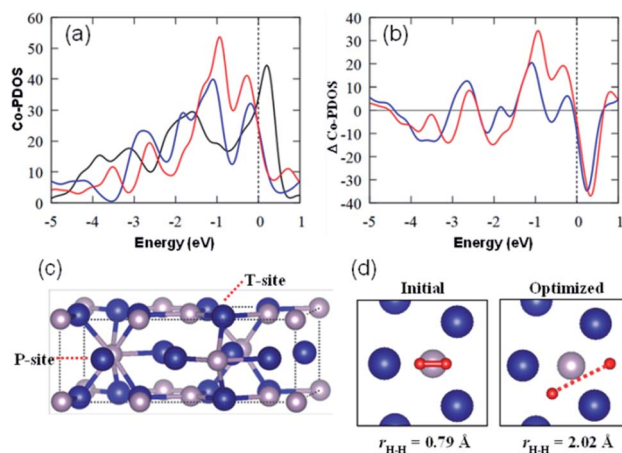
Fig. 6 (a) Projected density of states of the Co atom (Co-PDOS) in bulk Co (black), bulk Co_2P (blue) and on the Co_2P surface (red). (b) Differences of Co-PDOSs (ΔCo-PDOS) between bulk Co and bulk Co_2P (blue) and between the bulk Co and Co_2P surface (red). (c) Simulated unit cell of bulk Co_2P (Co in blue and P in pink). Co sites have tetrahedral (T) and pyramidal (P) geometries in the hexagonal Co_2P, and the DOSs of the Co atoms at T-site are shown in (a) and (b) (the others are in the ESI†). Fermi level is set to be zero. (d) Initial and optimized structures of the H_2 molecules on Co_2P (0001) T-site surface with the height of 1.2 Å and the distances between the hydrogen atoms (r_{H-H}). Several other structures are presented in the ESI†.

were purchased from Tokyo Chemical Industry Co., Ltd. Hydrotalcite (AD 500NS) was purchased from Tomita Pharmaceutical Co., Ltd. Al_2O_3 was purchased from Sumitomo Chemical. TiO_2 (JRC TIO-9) was provided by the Catalysis Society of Japan as a reference catalyst. SiO_2 (Q-9) was purchased from Fuji Silysia Chemicals Ltd. All nitriles were commercially available. Tokyo Chemical Industry Co., Ltd.: valeronitrile (>98%), decanenitrile (>98%), phenylacetonitrile (>98%), anisonitrile (>98%), 4-(trifluoromethyl)benzonitrile (>98%), methyl-4-cyanobenzoate (>98%), adiponitrile (>98%), sebaconitrile (98%), and isophthalonitrile (>98%). FUJIFILM Wako Pure Chemical: 1-adamantanecarbonitrile (97%), benzonitrile (>98%), 3-cyanopridine (>98%), 4-cyanopridine (>98%), 2-furancarbonitrile (98%), 5-cyanopridine (96%), 4-acetylbenzonitrile (>98%), and terephthalonitrile (>95%). Sigma-Aldrich: cyclohexanecarbonitrile (98%) and 4-bromobenzonitrile (99%).

Synthesis of nano-metal phosphides

All reactions were carried out under an argon atmosphere using standard Schlenk line techniques. In a typical synthesis, $CoCl_2 \cdot 6H_2O$ (1.0 mmol) and 2.4 g (10 mmol) of hexadecylamine were combined with 10.0 mL of 1-octadecene and 2.6 mL (10 mmol) of triphenyl phosphite in a Schlenk flask. The mixture was heated to 150 °C under an argon flow and maintained for 1 h. The temperature was then increased to 300 °C and kept at this temperature for 2 h, which yielded a black colloidal solution. The mixture was then cooled in air to room temperature. The obtained colloid was isolated by precipitation with acetone, and the redispersion and precipitation cycles continued using a chloroform and acetone mixed solvent (chloroform : acetone = 1 : 1) until the supernatant liquid was transparent. The obtained powder was dried in vacuum overnight at room temperature to give nano-Co_2P. The other nano-sized metal phosphides were prepared in a similar way to nano-Co_2P by using the corresponding metal precursors (Ni: $NiCl_2 \cdot 6H_2O$, Cu: $CuCl_2 \cdot 2H_2O$, and Fe: $Fe(CO)_5$).

Preparation of the nano-Co_2P/support

Typically, nano-Co_2P (0.04 g) was dispersed in hexane (50 mL) and stirred with hydrotalcite (1.0 g) for 2 h at room temperature. The obtained powder was dried in a vacuum overnight at room temperature to give nano-Co_2P/HT as a gray powder. The same procedure was used to prepare other nano-Co_2P/support catalysts (support = Al_2O_3, TiO_2 and SiO_2).

Synthesis of nano-CoP

In a typical synthesis, under a flow of argon, $Co(acac)_2$ (1 mmol), 1-octadecene (5 mL, 15.6 mmol) and oleylamine (10 mL, 30.4 mmol) were placed in a Schlenk flask. The mixture was stirred and heated to 120 °C and kept at this temperature for 1 h. Then, triphenylphosphine (5 mL, 11 mmol) was added to the above solution and heated to 340 °C for 4 h. Afterwards, the mixture was allowed to cool in air to room temperature. To remove as much organics as possible, redispersion and precipitation cycles continued until the supernatant liquid was transparent using a hexane and ethanol mixed solvent (hexane : ethanol =

1 : 1). The obtained powder was dried at room temperature in a vacuum overnight. The corresponding EDX spectrum revealed that the atomic ratio between Co and P was close to 1 : 1.

Preparation of CoO_x

All reactions were carried out under an argon atmosphere using standard Schlenk line techniques. Tri-n-octylphosphine oxide (0.1 g) and 0.09 g (0.32 mmol) of oleic acid were dissolved with 12 mL of 1,2-dichlorobenzene in a Schlenk flask. The mixture was heated to 180 °C under an argon flow and maintained for 10 min. 0.52 g (1.52 mmol) of $Co_2(CO)_8$ dissolved in 4 mL of 1,2-dichlorobenzene was quickly injected and stirred for 4 min. Afterwards, the mixture was allowed to cool in air to room temperature. The obtained powder was purified by using ethanol and centrifuged. Then the supernatant was removed and the powder was redispersed in hexane. The precipitation/redispersion process was performed twice overall.

Procedure for catalytic hydrogenation

A typical reaction procedure for the hydrogenation of nitrile using nano-Co_2P/HT was as follows. Nano-Co_2P/HT powder (0.1 g) was placed in a 50 mL stainless-steel autoclave with a Teflon inner cylinder, followed by addition of nitrile (0.5 mmol), 2-propanol (3 mL) and NH_3 aq. (25%, 1.2 mL). The reaction mixture was stirred vigorously at 130 °C under 40 bar of H_2. After the reaction, the reaction solution was analyzed by GC to determine the conversion and the yield using biphenyl as an internal standard. After reaction, to obtain the hydrochloride salts, the crude reaction mixture was filtered to remove the catalyst and the ammonia was removed under vacuum conditions. The mixture was then added to a hydrogen chloride solution (1.25 M, 1,4-dioxane). The solvent was removed leaving behind the corresponding salt, giving the pure hydrochloride salts, which were subjected to NMR analysis.

Characterization

Gas chromatography (GC-FID) and GC-mass spectrometry (GC-MS) were performed using a Shimadzu GC-2014 instrument equipped with an InertCap for amines (30 m × 0.32 mm i.d.) and a GCMS-QP2010 SE instrument equipped with an InertCap WAX-HT capillary column (30 m × 0.25 mm i.d.). The oven temperature was programmed as follows: 120 °C starting temperature, kept for 3 min, temperature ramp at 10 °C min^{-1} to 260 °C, then at -20 °C min^{-1} to 120 °C. Other conditions were as follows: 2.44 mL min^{-1} column flow rate, 10.0 split ratio; vaporization chamber temperature of 250 °C; detector temperature of 260 °C. ^1H and ^{13}C nuclear magnetic resonance (NMR) spectra were recorded using a JEOL JNM-ESC400 spectrometer. Transmission electron microscopy (TEM) observations were carried out using a JEM-ARM200F instrument operated at 200 kV. Scanning transmission electron microscopy (STEM) images with elemental maps were collected using a FEI Titan Cubed G2 60-300 instrument operated at 300 kV, and equipped with a Super-X energy-dispersive X-ray spectroscopy (EDX) detector. Elemental mapping based on quantification analysis of EDX spectra was carried out using Esprit. The TEM

sample and STEM sample were deposed without any pretreatment on a holey carbon supported Cu-grid (167 mesh. 30 μm thickness) and transferred to a microscope. Co K-edge X-ray absorption spectra were recorded at room temperature at the BL01B1 and BL14B2 lines, using a Si (311) or Si (111) monochromator, at SPring-8, Japan Synchrotron Radiation Research Institute (JASRI), Harima, Japan. Data analysis was performed using the REX 2000 program, ver. 2.5.7 (Rigaku). Fourier-transform infrared (FT-IR) spectra were recorded using a JASCO FT-IR 4100 spectrometer equipped with a mercury cadmium telluride detector. X-ray photoelectron spectroscopy (XPS) analyses were performed on an ESCA1700R system equipped with a dual Mg/Al X-ray source and a hemispherical analyzer operating in a fixed analyzer transmission mode. Spectra were obtained using a pass energy of 58.7 eV; an Al Kα X-ray source was operated at 350 W and 14 kV. Excess charges on the samples were neutralized by argon ion sputtering. The analysis area was 0.8×2 mm. The working pressure in the analyzing chamber was less than 1×10^{-7} Pa. Spectra were acquired in the Co 2p, P 2p, O 1s, C 1s, and Si 2p regions. The C 1s peak at a binding energy (BE) of 285 eV was taken as an internal reference.

Conflicts of interest

There are no conflicts to declare.

Acknowledgements

Notes and references

1 A. P. G. Kieboom, F. van Rantwijk and H. van Bekkum, *Hydrogenation and Hydrogenolysis in Synthetic Organic Chemistry*, Delft University Press, Delft, 1977.

2 J. Pritchard, G. Filonenko, R. Putten, E. Hensen and E. Pidko, *Chem. Soc. Rev.*, 2015, **44**, 3808–3833.

3 J. L. Legras, G. Chuzel, A. Arnaud and P. Galzy, *World J. Microbiol. Biotechnol.*, 1990, **6**, 83–108.

4 S. A. Lawrence, *Amines: Synthesis Properties, and Application*, Cambridge University Press, Cambridge, 2006.

5 S. D. Roughley and A. M. Jordan, *J. Med. Chem.*, 2011, **54**, 3451–3479.

6 S. Nishimura, *Handbook of Heterogeneous Catalytic Hydrogenation for Organic Synthesis*, Wiley-VCH, New York, 2001.

7 G. Ertl, H. Knözinger and J. Weitkamp, *Preparation of Solid Catalysts*, Wiley-VCH, New York, 1999.

8 P. Roose, K. Eller, E. Henkes, R. Rossbacher and H. Höke, *Amines, Aliphatic. Ullmann's Encyclopedia of Industrial Chemistry*, Wiley-VCH, New York, 2015.

9 L. Hegedűs and T. Máthé, *Appl. Catal., A*, 2005, **296**, 209–215.

10 M. Chatterjee, H. Kawanami, M. Sato, T. Ishizaka, T. Yokoyama and T. Suzuki, *Green Chem.*, 2010, **12**, 87–93.

11 M. Yoshimura, A. Komatsu, M. Niimura, Y. Takagi, T. Takahashi, S. Ueda, T. Ichikawa, Y. Kobayashi, Y. Monguchi and H. Sajiki, *Adv. Synth. Catal.*, 2018, **360**, 1726–1732.

12 D. Bagal and B. Bhanage, *Adv. Synth. Catal.*, 2015, **357**, 883–900.

13 R. Reguillo, M. Grellier, N. Vautravers, L. Vendier and S. Sabo-Etienne, *J. Am. Chem. Soc.*, 2010, **132**, 7854–7855.

14 M. Chatterjee, M. Sato, H. Kawanami, T. Yokoyama, T. Suzuki and T. Ishizaka, *Adv. Synth. Catal.*, 2010, **352**, 2394–2398.

15 K. Rajesh, B. Dudle, O. Blacque and H. Berke, *Adv. Synth. Catal.*, 2011, **353**, 1479–1484.

16 C. Chin and B. Lee, *Catal. Lett.*, 1992, **14**, 135.

17 C. Bornschein, S. Werkmeister, B. Wendt, H. Jiao, E. Alberico, W. Baumann, H. Junge and M. Beller, *Nat. Commun.*, 2014, **5**, 4111.

18 S. Chakraborty, G. Leitus and D. Milstein, *Chem. Commun.*, 2016, **52**, 1812–1815.

19 S. Lange, S. Elangovan, C. Cordes, A. Spannenberg, H. Jiao, H. Junge, S. Bachmann, M. Scalone, C. Topf, K. Junge and M. Beller, *Catal. Sci. Technol.*, 2016, **6**, 4768–4772.

20 R. Adam, C. Bheeter, J. Cabrero-Antonino, K. Junge, R. Jackstell and M. Beller, *ChemSusChem*, 2017, **10**, 842–846.

21 A. Mukherjee, D. Srimani, S. Chakraborty, Y. Ben-David and D. Milstein, *J. Am. Chem. Soc.*, 2015, **137**, 8888–8891.

22 S. Elangovan, C. Topf, S. Fischer, H. Jiao, A. Spannenberg, W. Baumann, R. Ludwig, K. Junge and M. Beller, *J. Am. Chem. Soc.*, 2016, **138**, 8809–8814.

23 K. Tokmic, B. Jackson, A. Salazar, T. Woods and A. Fout, *J. Am. Chem. Soc.*, 2017, **139**, 13554–13561.

24 H. Dai and H. Guan, *ACS Catal.*, 2018, **8**, 9125–9130.

25 J. Garduño and J. García, *ACS Catal.*, 2019, **9**, 392–401.

26 S. Weber, B. Stöger and K. Kirchner, *Org. Lett.*, 2018, **20**, 7212–7215.

27 F. Chen, C. Topf, J. Radnik, C. Kreyenschulte, H. Lund, M. Schneider, A. Surkus, L. He, K. Junge and M. Beller, *J. Am. Chem. Soc.*, 2016, **138**, 8781–8788.

28 R. Ferraccioli, D. Borovika, A. Surkus, C. Kreyenschulte, C. Topf and M. Beller, *Catal. Sci. Technol.*, 2018, **8**, 499–507.

29 Y. Zhang, H. Yang, Q. Chi and Z. Zhang, *ChemSusChem*, 2019, **12**, 1–11.

30 P. Ryabchuk, G. Agostini, M. Pohl, H. Lund, A. Agapova, H. Junge, K. Junge and M. Beller, *Sci. Adv.*, 2018, **4**, eaat0761.

31 K. Murugesan, T. Senthamarai, M. Sohail, A. Alshammari, M. Pohl, M. Beller and R. Jagadeesh, *Chem. Sci.*, 2018, **9**, 8553–8560.

32 J. Wang, Q. Tang, S. Jin, Y. Wang, Z. Yuan, Q. Chi and Z. Zhang, *New J. Chem.*, 2020, **44**, 549–555.

33 E. Popczun, J. McKone, C. Read, A. Biacchi, A. Wiltrout, N. Lewis and R. Schaak, *J. Am. Chem. Soc.*, 2013, **135**, 9267–9270.

34 S. Cao, Y. Chen, C. Wang, P. He and W. Fu, *Chem. Commun.*, 2014, **50**, 10427–10429.

35 Y. Shi and B. Zhang, *Chem. Soc. Rev.*, 2016, **45**, 1529–1541.

36 P. Liu and J. Rodriguez, *J. Am. Chem. Soc.*, 2005, **127**, 14871–14878.

37 T. Liu, D. Liu, F. Qu, D. Wang, L. Zhang, R. Ge, S. Hao, Y. Ma, G. Du, A. Asiri, L. Chen and X. Sun, *Adv. Energy Mater.*, 2017, **7**, 1700020.

38 S. T. Oyama, *J. Catal.*, 2003, **216**, 343–352.

39 Y. Lee and S. T. Oyama, *Appl. Catal., A*, 2017, **548**, 103–113.

40 P. Bui, S. T. Oyama, A. Takagaki, B. Carrow and K. Nozaki, *ACS Catal.*, 2016, **6**, 4549–4558.

41 A. Berenguer, T. M. Sankaranarayanan, G. Gómez, I. Moreno, J. M. Coronado, P. Pizarro and D. P. Serrano, *Green Chem.*, 2016, **18**, 1938–1951.

42 S. Yang, L. Peng, E. Oveisi, S. Bulut, D. Sun, M. Asgari, O. Trukhina and W. Queen, *Chem.Eur. J.*, 2018, **24**, 4234–4238.

43 K. Liu, Y. Wang, P. Chen, W. Zhong, Q. Liu, M. Li, Y. Wang, W. Wang, Z. Lu and D. Wang, *Appl. Catal., B*, 2016, **196**, 223–231.

44 R. Gao, L. Pan, H. Wang, X. Zhang, L. Wang and J. Zou, *ACS Catal.*, 2018, **8**, 8420–8429.

45 S. Carenco, A. Leyva-Pérez, P. Concepción and A. Corma, *Nano Today*, 2012, **7**, 21–28.

46 H. Feng, X. Li, H. Qian, Y. Zhang, D. Zhang, D. Zhao, S. Hong and N. Zhang, *Green Chem.*, 2019, **21**, 1743–1756.

47 J. Liu, Z. Wang, J. David, J. Llorca and A. Cabot, *J. Mater. Chem. A*, 2018, **6**, 11453–11462.

48 J. Liu, M. Meyns, T. Zhang, J. Arbiol, A. Cabot and A. Shavel, *Chem. Mater.*, 2018, **30**, 1799–1807.

49 A. Corma, S. Iborra and A. Velty, *Chem. Rev.*, 2007, **107**, 2411–2502.

50 K. Liu, C. Zhang, Y. Sun, G. Zhang, X. Shen, F. Zou, H. Zhang, Z. Wu, E. Wegener, C. Taubert, J. Miller, Z. Peng and Y. Zhu, *ACS Nano*, 2018, **12**, 158–167.

51 L. Zhou, C. Zhu, L. Edmonds, H. Yang, W. Cui and B. Li, *RSC Adv.*, 2014, **4**, 43220–43226.

52 F. A. G. Cotton, *Progress in Inorganic Chemistry: Metal–Metal Bonds in Transition Metal Compounds*, Wiley-VCH, New York, 1968.

53 Y. Chen, C. Li, J. Zhou, S. Zhang, D. Rao, S. He, M. Wei, D. Evans and X. Duan, *ACS Catal.*, 2015, **10**, 5756–5765.

54 C. D. Wagner, W. M. Riggs, L. E. Davis, J. F. Moulder and G. E. Muilenberg, *Handbook of X-Ray Photoelectron Spectroscopy*, Perkin-Elmer, Eden Prairie, 1979.

55 S. Cao, Y. Chen, C. Hou, X. Lv and W. Fu, *J. Mater. Chem. A*, 2015, **3**, 6096–6101.

56 J. Wang, L. Zhu, G. Dharan and G. Ho, *J. Mater. Chem. A*, 2017, **5**, 16580–16584.

57 A. Khassin, T. Yurieva, V. Kaichev, V. Bukhtiyarov, A. Budneva, E. Paukshtis and V. Parmon, *J. Mol. Catal. A: Chem.*, 2001, **175**, 189–204.

58 Z. Liang, X. Zhong, T. Li, M. Chen and G. Feng, *ChemElectroChem*, 2019, **6**, 260–267.

59 H. La Pierre, J. Arnold, R. Bergman and F. Dean Toste, *Inorg. Chem.*, 2012, **51**, 13334–13344.

60 Q. Chen, I.-H. Svenum, L. Gavrilovic, D. Chen and E. A. Blekkan, *Surf. Sci.*, 2019, **681**, 24–31.